2021 43rd Annual International Conference of the
IEEE Engineering in Medicine & Biology Society (EMBC)
Oct 31 - Nov 4, 2021. Virtual Conference

Graph Theoretic Analysis of Multilayer EEG Connectivity Networks

Zoe Dittman, Tamanna T. K. Munia and Selin Aviyente

Abstract— **Over the past twenty years, functional connectivity of the human brain has been studied in detail using tools from complex network theory. These methods include graph theoretic metrics ranging from the micro-scale such as the degree of a node to the macro-scale such as the small worldness of the brain network. However, most of these network models focus on average activity within a time window of interest and given frequency band. Therefore, they cannot capture the changes in network connectivity across time and different frequency bands. Recently, multilayer brain networks have attracted a lot of attention as they can capture the full view of neuronal connectivity. In this paper, we introduce a multilayer view of the functional connectivity network of the brain, where each layer corresponds to a different frequency band. We construct multi-frequency connectivity networks from electroencephalogram data where the intra-layer edges are quantified by phase synchrony while the inter-layer edges are quantified by phase-amplitude coupling. We then introduce multilayer degree, participation coefficient and clustering coefficient to quantify the centrality of nodes across frequency layers and to identify the importance of different frequency bands. The proposed framework is applied to electroencephalogram data collected during a study of error monitoring in the human brain.**

I. INTRODUCTION

The human brain is widely considered to be a complex network that can be studied by graph theoretical approaches. In such a description, nodes in the network correspond to anatomical regions and links typically refer to either structural or functional connections between those regions. Graph theory has been applied successfully to networks derived from a wide range of modalities and for a variety of cognitive tasks [1]. Various metrics, describing both local and global topological network characteristics, have been shown to provide useful quantitative descriptions of networks in order to differentiate between brain states during cognitive tasks [2]. Despite its promise, most of the application of graph theory to neuroimaging studies has been limited to studying single layer networks that correspond to the average connectivity for a given modality and within a time window and frequency band of interest.

Recently, multilayer network approaches have been introduced to the field of neuroscience [3], [4], [5], [6], where different layers can correspond to different modalities, time points or frequency bands. A multilayer network can be considered as a 'network of networks', which consists of individual network layers that are interconnected and where a given node can be involved in different types of interactions [7], [8], [9].

This work was in part supported by NSF CCF 2006800.

Z. Dittman, T. T. K. Munia and S. Aviyente are with the Department of Electrical and Computer Engineering, Michigan State University, East Lansing, MI 48824, USA

It is well-known that for electroencephalogram (EEG), synchronization within different frequency bands and cross-frequency coupling play a major role in many internal cognitive processes like decision making, memory and error processing. Thus, there is no reason why different frequency-specific networks would operate independently from one another [3], [4]. For this reason, in this paper, we will present a multilayer view of functional connectivity networks, where each layer corresponds to a different frequency band.

Despite the promise of this multilayer network view of the brain, there is a lack of graph theoretic metrics that can characterize the topology of fully connected multilayer networks. Most of the extensions of graph theoretic metrics to multilayer networks are limited to multiplex networks, where the only inter-layer connections are between a node and its replica across layers [7], [10]. Thus, they cannot distinguish between the centrality of a particular node within a layer versus across layers, i.e., differentiate between brain regions that play a key role within a frequency band versus brain regions that are central to cross-frequency coupling.

In this paper, we address these issues by first introducing a methodology for constructing multilayer functional connectivity networks from EEG data, where each layer corresponds to a different frequency band. The intra-layer edges are quantified through a measure of phase synchrony, while the inter-layer edges are quantified through a measure of cross-frequency phase-amplitude coupling (PAC). After the multilayer networks are constructed, we introduce multilayer centrality metrics, i.e., degree, clustering coefficient and participation coefficient. These metrics are extensions of conventional graph theoretic metrics defined for single layer networks and are defined for both intra- and inter-layer networks. Finally, the proposed framework is applied to EEG recordings collected during a cognitive control study to determine the brain regions that are central to error processing across different frequency bands.

II. BACKGROUND

A. Reduced Interference Rihaczek (RID-Rihaczek) Time-Frequency Distribution

RID-Rihaczek distribution of a signal $x(t)$ is defined as [11]:

$$C(t,f) = \int\int \exp\left(-\frac{(\theta\tau)^2}{\sigma}\right)\exp\left(j\frac{\theta\tau}{2}\right)A(\theta,\tau)e^{-j(\theta t+2\pi f\tau)}d\tau d\theta, \quad (1)$$

where $\exp\left(-\frac{(\theta\tau)^2}{\sigma}\right)$ corresponds to the Choi-Williams kernel with the variance parameter σ, and $\exp\left(j\frac{\theta\tau}{2}\right)$ corresponds to the kernel function of the Rihaczek distribution [12], $A(\theta,\tau)$

978-1-7281-1178-0/21/$31.00 ©2021 IEEE

refers to the ambiguity function of a signal $x(t)$ and is defined as:

$$A(\theta,\tau)=\int x\big(u+\frac{\tau}{2}\big)x^{*}\big(u-\frac{\tau}{2}\big)e^{j\theta u}du. \tag{2}$$

This complex time-frequency distribution can be used to extract the amplitude and phase components of a given signal.

B. Intra-layer Coupling Measure

In this paper, the intra-layer edges, i.e., within frequency band connectivities, are quantified using time-frequency phase synchrony (TFPS) measure based on RID-Rihaczek time-frequency distribution [11], [13]. Based on the complex distribution defined in (1), the instantaneous phase of a signal $x_i(t)$ is computed as:

$$\phi_i(t,f)=\arg\left[\frac{C_i(t,f)}{|C_i(t,f)|}\right], \tag{3}$$

and the phase difference, $\phi_{i,j}(t,f)$, between two signals $x_i(t)$ and $x_j(t)$, recorded from electrodes i and j can be computed as:

$$\phi_{i,j}(t,f)=\arg\left[\frac{C_i(t,f)C_j^{*}(t,f)}{|C_i(t,f)||C_j(t,f)|}\right]. \tag{4}$$

Phase Locking Value (PLV) is defined as the consistency of the phase differences $\phi_{i,j}(t,f)$ across trials and can be computed as:

$$PLV_{i,j}(t,f)=\frac{1}{K}\left|\sum_{k=1}^{K}\exp\big(j\phi_{i,j}^{k}(t,f)\big)\right|, \tag{5}$$

where K is the total number of trials and $\phi_{i,j}^{k}(t,f)$ is the phase difference for the kth trial. Once the pairwise PLV values are computed between all pairs of brain regions, this pairwise synchrony is used to construct the intra-layer adjacency matrix for the lth frequency band, i.e., $\mathbf{A}_{i,j}^{l}=\frac{\sum_{t\in T}\sum_{f\in F_l}PLV_{i,j}(t,f)}{|T|.|F_l|}$, $1\le i,j\le n$, where T is the time window of interest, $|T|$ is the length of this time window, $|F_l|$ is the number of frequency bins in the lth frequency band, F_l, and n is the number of brain regions.

C. Inter-layer Coupling Measure

The inter-layer edges, i.e., cross-frequency connectivities, are quantified by PAC, which quantifies the modulation of the amplitude of a high frequency oscillation by the phase of a slow rhythm [14], [15]. PAC between two brain regions is quantified using the RID-Rihaczek time-frequency based PAC measure [16], [17]. RID-Rihaczek distribution is used to extract both the envelope of the high frequency amplitude component at electrode i, $A_{f_a}^{i}(t)$, and the low frequency phase component at electrode j, $\phi_{f_p}^{j}(t)$, where f_a and f_p are frequencies within the lth and mth frequency bands, respectively. $A_{f_a}^{i}(t)$ is extracted from the RID-Rihaczek distribution, $C_i(t,f)$, by computing a frequency constrained time marginal as follows:

$$A_{f_a}^{i}(t)=\int_{f_{a_1}}^{f_{a_2}}C_i(t,f)df, \tag{6}$$

where f_{a_1} and f_{a_2} define the bandwidth around the high frequency of interest. The phase of the low frequency signal at f_p is extracted from RID-Rihaczek distribution $C_j(t,f)$ similar to (3). After detecting the amplitude and phase, PAC is computed by mapping the amplitude time series $A_{f_a}^{i}(t)$ and phase time series $\phi_{f_p}^{j}(t)$ to a complex-valued vector at each time point and computing the amplitude normalized modulation index (MI) [18] as follows:

$$MI_{i,j}(f_p,f_a,t)=\frac{1}{\sqrt{K}}\frac{\left|\sum_{k=1}^{K}A_{f_a}^{i,k}(t)e^{j\phi_{f_p}^{j,k}(t)}\right|}{\sqrt{\sum_{k=1}^{K}A_{f_a}^{i,k}(t)^{2}}}, \tag{7}$$

where K is the number of trials. The value of MI ranges between 0 and 1 as it is amplitude-normalized [19]. MI can be used to construct the inter-layer adjacency matrix as $\mathbf{H}_{i,j}^{l,m}=\frac{\sum_{t\in T}\sum_{fp\in F_l}\sum_{fa\in F_m}MI_{i,j}(f_p,f_a,t)}{|F_l|.|F_m|.|T|}$, where T is the time window of interest, $|F_l|$ is the number of frequency bins in the lth frequency band and $|F_m|$ is the number of frequency bins in the mth frequency band.

III. MATERIALS AND METHODS

A. EEG Data Acquisition

In this paper, we analyze EEG data collected during a cognitive control-related error processing study. The experimental procedures involving human subjects described in this paper were approved by the MSU Institutional Review Board. The Institution's Ethical Review Board approved all experimental procedures involving human subjects. Participants were recruited from Michigan State University campus, greater Lansing and East Lansing communities. All of them were female and the mean age was 20.78 (SD = 1.81). A letter version of the speeded reaction Flanker task [20] was performed. For each trial, a string of five letters, which could be congruent (e.g., SSSSS) or incongruent stimuli (e.g., SSTSS), were presented to each participant. The participants were instructed to select the center letter with a standard mouse with respect to the Flanker letters. Each trial began with 35ms of flanking stimuli (e.g., SS SS). After that, the target stimuli were presented for 100 ms (total presentation time is 135ms) by embedding them in the center of the flanker letters (e.g., SSSSS/SSTSS) followed by an inter-trial random interval ranging from 1200 to 1700 ms. The EEG was recorded using the ActiveTwo system (BioSemi, Amsterdam, The Netherlands). 64 Ag–AgCl electrodes were placed following the international 10/20 system. The sampling frequency of the data was 512 Hz. Trials with artifacts were removed and Current Source Density (CSD) Toolbox [21] was used to minimize the volume conduction. Each trial was one second long. The trials corresponding to the error responses were considered for multi-frequency functional connectivity analysis. EEG data from 20 participants were considered for this analysis. The inclusion criteria was that the number of trials for error response should be at least 40.

B. Multilayer Networks

A multilayer network with M layers can be defined as a quadruplet $\mathscr{M} = (V_{\mathscr{M}}, E_{\mathscr{M}}, V, \mathbf{L})$, where V and $\mathbf{L}$ represent the set of objects and the set of layers with cardinalities $|V| = n$ and $|\mathbf{L}| = M$, respectively [9]. $V_{\mathscr{M}}$ and $E_{\mathscr{M}}$ are the set of nodes and edges, respectively where $V_{\mathscr{M}} = \{V^l_{\mathscr{M}} : V^l_{\mathscr{M}} \in V, l \in \mathbf{L}\}$ with $V^l_{\mathscr{M}}$ as the set of nodes in layer l and $E_{\mathscr{M}} = \{e^{l,m}_{uv} : u^l, v^m \in V_{\mathscr{M}}\}$ with $e^{l,m}_{uv}$ as the set of edges between the uth and vth nodes in lth and mth layers, respectively.

Simple graphs can be constructed from $V_{\mathscr{M}}$ and $E_{\mathscr{M}}$. In particular, intra-layer and inter-layer networks can be defined as $G^l_{\mathscr{M}} = (V^l_{\mathscr{M}}, E^l_{\mathscr{M}})$ and $G^{l,m}_{\mathscr{M}} = (V^l_{\mathscr{M}} \cup V^m_{\mathscr{M}}, E^{l,m}_{\mathscr{M}})$, respectively. Finally, adjacency matrices of these simple networks are denoted as $\mathbf{A}^l \in \mathbb{R}^{n_l \times n_l}$ and $\mathbf{H}^{l,m} \in \mathbb{R}^{n_l \times n_m}$, respectively. In this paper, we focus on node-aligned multilayer networks (fully connected) where all the layers contain all of the nodes, i.e., $n_l = n$. These intra- and inter-layer adjacency matrices can be used to construct the *supra-adjacency* matrix, $\mathbf{A}_{Supra}$, of the multilayer network, $\mathscr{M}$, as:

$$\mathbf{A}_{Supra} = \begin{bmatrix} \mathbf{A}^1 & \mathbf{H}^{1,2} & \dots & \mathbf{H}^{1,M} \\ \mathbf{H}^{2,1} & \mathbf{A}^2 & \dots & \mathbf{H}^{2,M} \\ \vdots & \ddots & \ddots & \vdots \\ \mathbf{H}^{M,1} & \mathbf{H}^{M,2} & \dots & \mathbf{A}^M \end{bmatrix}. \tag{8}$$

C. Multilayer Degree

Using the supra-adjacency matrix, we can define both the total degree of each node i in the supra-adjacency matrix as well as intra- and inter-layer degree. The total degree of node i, d_i, is defined as the sum of the weights of all edges connected to that node both within the layer and across other layers as follows:

$$d_i = \sum_{l=1}^{M} \sum_{m=1}^{M} \sum_{j=1}^{n} e^{l,m}_{ij}, \tag{9}$$

assuming $e^l_{ii} = 0$.

We define the intra-layer degree of node i for layer l, d^l_i, as:

$$d^l_i = \sum_{j=1}^{n} e^l_{ij}. \tag{10}$$

Finally, we define the inter-layer degree of each node i with respect to layer l, $\bar{d}^l_i$, as:

$$\bar{d}^l_i = \sum_{l \neq m} \sum_{j=1}^{n} e^{l,m}_{ij}. \tag{11}$$

D. Multilayer Participation Coefficient

In this paper, we define participation coefficients to quantify the contribution of each node to each layer of the network. Unlike participation coefficient for a multiplex network [10], in this paper, we compute two different types of participation coefficient; intra-layer participation coefficient, Pw^l_i, and inter-layer participation coefficient, Pa^l_i, as:

$$\begin{aligned} Pw^l_i &= n\frac{d^l_i}{d^l}, \\ Pa^l_i &= n\frac{\bar{d}^l_i}{\bar{d}^l}, \end{aligned} \tag{12}$$

where d^l and $\bar{d}^l$ are the total intra- and inter-layer degrees for layer l, respectively. Pw^l_i quantifies how much a particular node contributes to a layer's intra-layer degree while Pa^l_i quantifies how much a particular node contributes to a layer's inter-layer degree. If this metric is greater than 1, it implies that the particular node contributes more than the total degree partitioned uniformly across nodes and vice versa.

E. Multilayer Clustering Coefficient

The clustering coefficient quantifies the degree to which neighboring nodes in a network form a cluster [22]. The clustering coefficient of node i is the average "intensity" of all triangles associated with that node, and is in the range $[0,1]$. In this paper, we computed two different types of clustering coefficient; intra-layer clustering coefficient, C^l_i, and inter-layer clustering coefficient, $\bar{C}^l_i$:

$$\begin{aligned} C^l_i &= \frac{1}{d^l_i(d^l_i - 1)} \sum_{j,k} e^l_{ij} e^l_{jk} e^l_{ki}, \\ \bar{C}^l_i &= \frac{1}{\bar{d}^l_i(\bar{d}^l_i - 1)} \sum_{j,k} \bar{e}^l_{ij} \bar{e}^l_{jk} \bar{e}^l_{ki}, \end{aligned} \tag{13}$$

where $\bar{e}^l_{ij} = \frac{1}{M-1} \sum_{m \neq l} e^{l,m}_{ij}$. Therefore, the intra-layer clustering coefficient computes the local clustering coefficient of each node within a layer without taking any of the other layers into account whereas the inter-layer clustering coefficient of a node is computed with respect to the average inter-layer edge strength.

F. Feature Extraction

For each intra- and inter-layer adjacency matrix, we extracted three different features per node, namely degree, participation coefficient and clustering coefficient. In order to identify the nodes that are central for each frequency band and across all subjects, we first form the feature matrix $X \in \mathbb{R}^{n \times 3S}$, where S is the number of subjects. We extract the principal components from each feature matrix corresponding to each frequency band by first computing the covariance matrix $\Sigma = XX^T$ and then computing its eigendecomposition $\Sigma = U\Gamma U^T$, where Γ is a diagonal matrix of the eigenvalues and U is a unitary matrix corresponding to the eigenvectors. Based on the distribution of the eigenvalues, we use the z-scores of the entries of the first eigenvector to identify central nodes.

IV. RESULTS

In this paper, we constructed multilayer networks for each subject where each layer corresponds to a different frequency band. In particular, we considered four frequency bands: θ (4-7 Hz), α (8-12 Hz) , β (13-30 Hz), γ (31-100 Hz). For each multilayer network, we computed the different metrics both within and across layers, e.g., intra and inter-layer degree, participation coefficient and clustering coefficient. For each subject, this resulted in 8 feature matrices, 4 corresponding to each frequency band and 4 corresponding to each frequency band's interactions with other frequency bands.

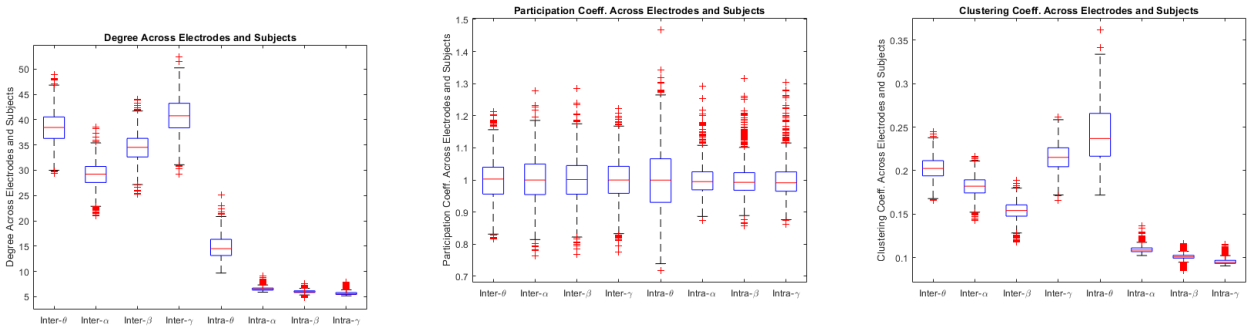

(a) Distribution of degree across electrodes and subjects by frequency band

(b) Distribution of participation coefficient across electrodes and subjects by frequency band

(c) Distribution of clustering coefficient across electrodes and subjects by frequency band

Fig. 1: Box plots representing three different metrics: degree, participation, clustering coefficient, averaged across electrodes and subjects by frequency band.

For each of the three different metrics we calculated (degree, participation, and clustering coefficient), the box plots for the different frequency bands are shown in Fig. 1. These box plots represent the distribution of each metric computed within or between frequency bands across subjects and electrodes. These plots illustrate the importance of the different frequency bands and the discriminative power of the different metrics. It can be seen from this figure that the degree and clustering coefficient are more discriminative across the frequency bands compared to the participation coefficient. In particular, all of the pairwise intra- and inter-frequency band comparisons were significant at $\alpha = 0.01$ (Bonferroni corrected, using Wilcoxon ranksum test) for the degree and clustering coefficient metrics. The participation coefficient, on the other hand, did not yield any significant differences across frequency bands. From the multilayer degree and clustering coefficient, it can be seen that inter-layer connections between theta and gamma bands are stronger, i.e., higher degree and clustering coefficient, compared to the other frequency bands. This is consistent with prior studies where PAC was reported between theta phase and gamma amplitude for visual tasks like working memory processing and serial memory recall [15]. Significant theta-gamma PAC during error response was also reported in an error processing study [23]. It is hypothesized that large-scale functional integration across different frequency bands supports flexible behavior adaption to improve the performance after an error and thus results in an increase of PAC following error response. Comparing intra-layer connections, it can be seen that theta frequency band has stronger connections than the other frequency bands. This is in line with previous research on error monitoring showing increased synchronization for theta band [13].

For each of the frequency bands, we also investigated the centrality of different brain regions. From the eight feature matrices corresponding to the different frequency bands, we computed the first eigenvector of the covariance matrix and found the z-scores for the first eigenvector. These z-scores were used to identify the electrodes that are significant for each frequency band at the 90% (orange), 95% (yellow) and the 98% (green) significance levels. The topomaps illustrating the significant electrodes for each frequency band can be seen in Fig. 2.

It can be seen that for θ-band, the significant electrodes are in the frontal-central regions consistent with previous findings on θ-band synchronization during error monitoring [24], [13]. Similarly, intra β and γ synchronization are concentrated in the frontal region, while there is no localization for α-band activity. With respect to inter-layer centrality, parietal-occipital regions are found to be central for both θ and γ bands. This indicates the presence of theta-gamma coupling between these brain regions. Similarly, there is some overlap between α and β bands in terms of the brain regions that are responsible for cross-frequency coupling.

V. CONCLUSIONS

In this paper, we presented a multilayer network approach to studying functional connectivity of the brain. We constructed a multi-frequency network from EEG and developed multilayer graph theoretic metrics. These metrics are used to identify the central nodes within and across frequency bands as well as illustrate the importance of different frequency bands. The application to EEG data from a study of error monitoring in the brain illustrated that with this approach, we can differentiate across frequency bands in terms of their contributions to error processing. We identified that theta band synchronization as well as theta-gamma coupling play an important role in the functional connectivity network for error monitoring. These metrics also help us differentiate between brain regions that are key to functional integration within and across frequency layers. In particular, we identify that frontal-central regions play a key role in theta band synchronization while parietal-occipital regions play a role in theta-gamma coupling.

ACKNOWLEDGMENT

The authors would like to thank Dr. J. S. Moser from Michigan State University for providing the EEG data.

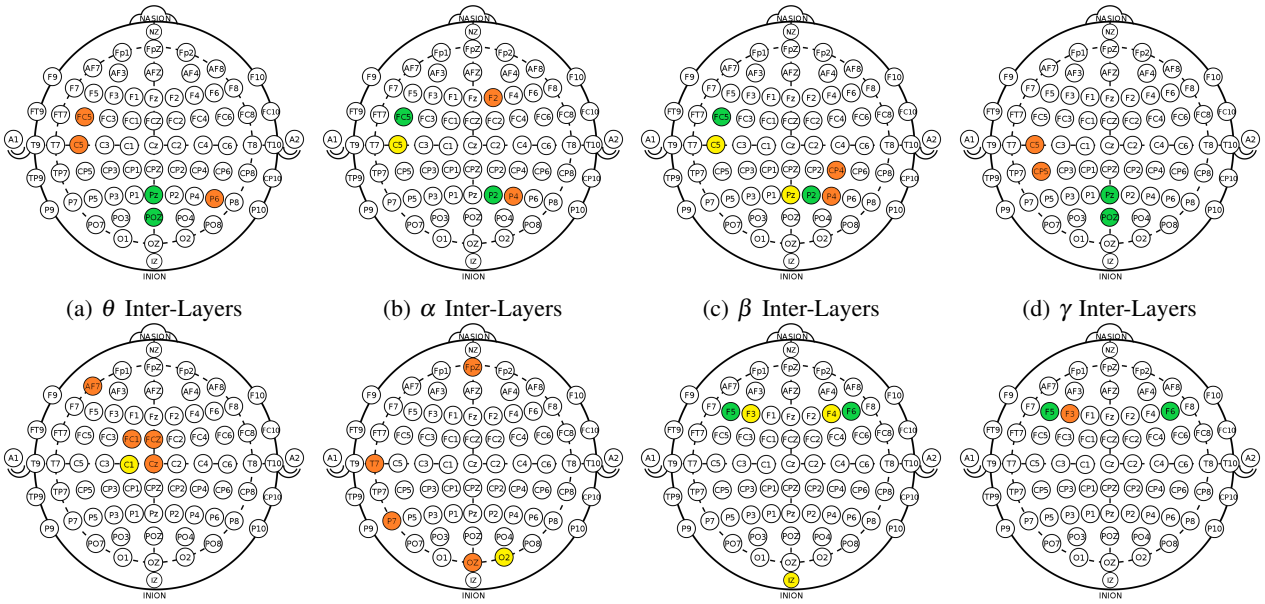

(a) θ Inter-Layers (b) α Inter-Layers (c) β Inter-Layers (d) γ Inter-Layers

(e) θ Intra-Layers (f) α Intra-Layers (g) β Intra-Layers (h) γ Intra-Layers

Fig. 2: Significant electrodes based on z-scores of the first eigenvector of the feature matrices. The different colors indicate the significance levels for each electrode (orange: 90%, yellow: 95% and green: 98%).

REFERENCES

[1] O. Sporns, "Graph theory methods: applications in brain networks," *Dialogues in clinical neuroscience*, vol. 20, no. 2, p. 111, 2018.

[2] U. Braun, A. Schäfer, D. S. Bassett, F. Rausch, J. I. Schweiger, E. Bilek, S. Erk, N. Romanczuk-Seiferth, O. Grimm, L. S. Geiger *et al.*, "Dynamic brain network reconfiguration as a potential schizophrenia genetic risk mechanism modulated by nmda receptor function," *Proceedings of the National Academy of Sciences*, vol. 113, no. 44, pp. 12 568–12 573, 2016.

[3] M. J. Brookes, P. K. Tewarie, B. A. Hunt, S. E. Robson, L. E. Gascoyne, E. B. Liddle, P. F. Liddle, and P. G. Morris, "A multi-layer network approach to meg connectivity analysis," *Neuroimage*, vol. 132, pp. 425–438, 2016.

[4] P. Tewarie, A. Hillebrand, B. W. van Dijk, C. J. Stam, G. C. O'Neill, P. Van Mieghem, J. M. Meier, M. W. Woolrich, P. G. Morris, and M. J. Brookes, "Integrating cross-frequency and within band functional networks in resting-state meg: a multi-layer network approach," *Neuroimage*, vol. 142, pp. 324–336, 2016.

[5] J. M. Buldú and M. A. Porter, "Frequency-based brain networks: From a multiplex framework to a full multilayer description," *Network Neuroscience*, vol. 2, no. 4, pp. 418–441, 2018.

[6] M. De Domenico, S. Sasai, and A. Arenas, "Mapping multiplex hubs in human functional brain networks," *Frontiers in neuroscience*, vol. 10, p. 326, 2016.

[7] S. Boccaletti, G. Bianconi, R. Criado, C. I. Del Genio, J. Gómez-Gardenes, M. Romance, I. Sendina-Nadal, Z. Wang, and M. Zanin, "The structure and dynamics of multilayer networks," *Physics reports*, vol. 544, no. 1, pp. 1–122, 2014.

[8] P. Van Mieghem, "Interconnectivity structure of a general interdependent network," *Physical Review E*, vol. 93, no. 4, p. 042305, 2016.

[9] M. Kivelä, A. Arenas, M. Barthelemy, J. P. Gleeson, Y. Moreno, and M. A. Porter, "Multilayer networks," *Journal of complex networks*, vol. 2, no. 3, pp. 203–271, 2014.

[10] F. Battiston, V. Nicosia, and V. Latora, "Structural measures for multiplex networks," *Physical Review E*, vol. 89, no. 3, p. 032804, 2014.

[11] S. Aviyente and A. Y. Mutlu, "A time-frequency-based approach to phase and phase synchrony estimation," *IEEE Transactions on Signal Processing*, vol. 59, no. 7, pp. 3086–3098, 2011.

[12] A. W. Rihaczek, "Signal energy distribution in time and frequency," *IEEE Transaction on information Theory*, vol. 14, no. 3, pp. 369–374, 1968.

[13] S. Aviyente, E. Bernat, W. Evans, and S. Sponheim, "A phase synchrony measure for quantifying dynamic functional integration in the brain," *Human Brain Mapping*, vol. 32, no. 1, pp. 80–93, 2011.

[14] A. Bragin, G. Jandó, Z. Nádasdy, J. Hetke, K. Wise, and G. Buzsáki, "Gamma (40-100 hz) oscillation in the hippocampus of the behaving rat," *Journal of neuroscience*, vol. 15, no. 1, pp. 47–60, 1995.

[15] A. B. Tort, R. Komorowski, H. Eichenbaum, and N. Kopell, "Measuring phase-amplitude coupling between neuronal oscillations of different frequencies," *Journal of neurophysiology*, vol. 104, no. 2, pp. 1195–1210, 2010.

[16] T. T. Munia and S. Aviyente, "Time-frequency based phase-amplitude coupling measure for neuronal oscillations," *Scientific reports*, vol. 9, no. 1, pp. 1–15, 2019.

[17] T. T. K. Munia and S. Aviyente, "Comparison of wavelet and ridrihaczek based methods for phase-amplitude coupling," *IEEE Signal Processing Letters*, vol. 26, no. 12, pp. 1897–1901, 2019.

[18] T. E. Özkurt and A. Schnitzler, "A critical note on the definition of phase–amplitude cross-frequency coupling," *Journal of Neuroscience methods*, vol. 201, no. 2, pp. 438–443, 2011.

[19] M. J. Hülsemann, E. Naumann, and B. Rasch, "Quantification of phase-amplitude coupling in neuronal oscillations: comparison of phase-locking value, mean vector length, modulation index, and generalized-linear-modeling-cross-frequency-coupling," *Frontiers in neuroscience*, vol. 13, p. 573, 2019.

[20] T. P. Moran, D. Taylor, and J. S. Moser, "Sex moderates the relationship between worry and performance monitoring brain activity in undergraduates," *International Journal of Psychophysiology*, vol. 85, no. 2, pp. 188–194, 2012.

[21] C. E. Tenke and J. Kayser, "Generator localization by current source density (csd): implications of volume conduction and field closure at intracranial and scalp resolutions," *Clinical neurophysiology*, vol. 123, no. 12, pp. 2328–2345, 2012.

[22] J. Saramäki, M. Kivelä, J.-P. Onnela, K. Kaski, and J. Kertesz, "Generalizations of the clustering coefficient to weighted complex networks," *Physical Review E*, vol. 75, no. 2, p. 027105, 2007.

[23] M. X. Cohen and S. Van Gaal, "Dynamic interactions between large-scale brain networks predict behavioral adaptation after perceptual errors," *Cerebral Cortex*, vol. 23, no. 5, pp. 1061–1072, 2013.

[24] J. F. Cavanagh, M. X. Cohen, and J. J. Allen, "Prelude to and resolution of an error: Eeg phase synchrony reveals cognitive control dynamics during action monitoring," *Journal of Neuroscience*, vol. 29, no. 1, pp. 98–105, 2009.